JMechE, Vol.8, Issue 2:71-91 (2011)

Impact Response of Multi Slotted Square Column

Amir Radzi Ab. Ghani
Faculty of Mechanical Engineering, Universiti Teknologi MARA,
40450 Shah Alam, Selangor, MALAYSIA
amirradzi@gmail.com

M.A. Hassan and M.Hamdi
Department of Engineering Design & Manufacture,
Faculty of Engineering, University of Malaya,
50603 Kuala Lumpur, MALAYSIA

Zahari Taha
Faculty of Mechanical Engineering, Universiti Malaysia Pahang,
26300 Kuantan, Pahang, MALAYSIA

ABSTRACT

This work investigates the impact response of multi slotted square hollow section column. Abaqus Explicit finite element code was used to simulate the response of this structure subjected to varying impact speeds. A comparative study with the standard plain square column was carried out and it was found that the slotted column exhibited lower initial peak force (IPF) as compared to the plain column. Mean forces for both types of columns remained the same. Both types of columns exhibited different IPFs with different impact speeds. The number of slots on the slotted column also influenced the formation of folds during the progressive crushing. The low IPF is an important feature when designing for occupant and critical goods safety. Based on these preliminary findings, it is believed that impact performance of standard square column can be improved over a wider range of impact speeds and impact mass by correct placement of slots.

Keywords*: Structural crashworthiness, impact response, square column, non-linear explicit finite element*

Introduction

Crashworthiness is the measure of performance of vehicles during collisions. The aims of structural crashworthiness are to minimise the load and deceleration of the vehicles and occupants and to disperse the kinetic energy resulting from the impact event [1]. Energy absorbers in the form of columns and frustas of various shapes and sizes are mainly used for impact protection. Ductile materials such as steels and aluminium are the preferred choice as they exhibit large plastic deformation before total fracture. These materials absorb the excessive kinetic energy during impact by various mechanisms such as friction, fracture, shearing, bending, tension, crushing and plastic deformation.

Widely used geometries such as square and circular tubes, frustas and polygons subjected to axial and lateral loadings have been extensively studied for the past five decades [2,3]. The need to further optimise the structures has prompted researchers to experiment with new geometries, configurations and material combinations. Zhang and Cheng [4] carried out comparative studies of energy absorption characteristics of foam filled and multi cell column. Both foam filled and multi cell columns exhibited higher energy absorption as compared to plain columns. In the foam filled column, foam filler acted as a semi-elastic foundation for the sidewall which resulted in decreasing buckling length of sidewall and thus higher plastic deformations and buckling load. In the multi-cell column, the additional bending and stretching of inner cell faces plus the main four faces contribute to the increase of energy absorption. However, the additional stiffness resulted in a high initial peak force (IPF) which can cause injury to the occupants. The incorporation of a trigger mechanism by means of a groove managed to reduce the high IPF while maintaining the energy absorption performance.

Daneshi, G.H and Hosseinipou, S.J. [5] carried out experimental work on grooved thin walled tubes subjected to axial compression. The function of the groove in the tube is to force the plastic deformation to occur at predetermined intervals along the tube. The aims were to improve the uniformity of the load-displacement behaviour and better predict the energy absorption capacity of the tubes. Quassi-static axial crushing tests were performed with different groove distance. The results showed favourable characteristics where the grooved tubes exhibited lower initial peak loads and more uniform and stable crushing modes and mean loads.

Zhang, X. et al [6] carried out numerical investigation on a new tube configuration called retractable/telescopic tube; straight retractable (SR) and tapered retractable (TR), subjected to axial crushing. The inversion process of the proposed tubes under axial crushing was simulated by using the non-linear finite element code LS-Dyna. A comparative study based on the performance indices used most commonly for energy absorbing devices, of the energy absorption characteristics of the proposed tubes with the plain circular tube was conducted. The results showed that the proposed

tubes outperformed the plain circular tube in almost every aspects of performance indices (lower peak force and higher crush force efficiency (CFE) and specific total efficiency (STE)), except the specific energy absorption (SEA). In addition, a parametric study was carried out to investigate the effects of the geometric parameters on the behaviour of the retractable tubes. It was discovered that the behaviour of SR tubes is greatly influenced by the width of the annular connection zone, while the behaviour of the TR tubes is found to be insensitive. A three-level retractable tube was also tested and it was found to have an even better performance. Mathematical model of the TR tube has yet to be developed and therefore further research needs to be done.

Zhang, X.W. et al. [7] studied the effect of a buckling initiator on the response of an axially crushed square tube. The buckling initiator consisted of a pre-hit column with pulling strips attached to both sides of the inner tube near the impacted end. When subjected to axial impact, the pre-hit column will be hit by the striker first which will cause the strips to pull the two opposite walls of the tube, creating some geometric imperfections. The results showed a considerable decrease in IPF while little effect was observed on the mean force and deformation mode. The reduction of peak force was found to be greatly influenced by the pre-hit height. To minimize the length and maximize the effective stroke of the tube, the pulling strips must be positioned as close as possible to the top edge of the tube. Added advantages of this system are stiffness of the intact square tube in its normal structural function is maintained and a more stable and uniform crushing mode is ensured. A simplified analytical model to relate the reduction of peak load with the geometric imperfection was developed. The model was able to predict the effectiveness of the buckling initiator to a certain extent.

From previous researches, it can be deduced that a particular structure configuration is most efficient in absorbing the impact energy for a specific load, speed and direction. In the real world, it would be more relevant to design a structure that can efficiently absorb the impact energy over a wide range of conditions while at the same time having lower IPF to reduce occupant injury. Current researches explore the use of trigger mechanism incorporated in structures that aims to induce failure in a desired manner and having impact response which are optimized for a wide range of conditions.

Impact Performance Indices

Crashworthiness of a structure can be expressed in term of specific energy absorption (SEA), E_s which is the ratio of energy absorbed to the unit mass of the material. It allows direct comparison of similiarly shaped structures made from different materials.

$$E_s = \frac{W}{V\rho} \tag{1}$$

where W = total energy absorbed

V = volume of material

ρ = density of material

Crush force efficiency (CFE), η_c is the useful measure of the uniformity of collapse force. It is defined as the ratio of mean load, F_{mean} to initial peak force, F_{peak}. An ideal absorber is said to exhibit a crush force efficiency of 100% which is difficult to achieve in reality.

$$\eta_C = \frac{F_{mean}}{F_{peak}} \tag{2}$$

The initial peak force (IPF) is also of equal importance as this force tends to be very high and may cause severe injury to the occupant. In some structures, trigger mechanism is added to the existing system as a mean to reduce the high initial peak force, and henceforth, the addition of slot in this work.

Finite Element Modelling

The plain square column was chosen as the object of study. Its ease of fabrication, versatility and superior impact energy absorption enables it to be widely used in automotive structures. Even though most modern automotive structures consist of highly complicated shapes and configurations, energy absorbers in the form of square column and its derivatives are predominantly used to withstand the frontal collision.

The plain square column was modeled in Abaqus as a 3D deformable shell. The bottom plate which represents the support and the top plate which represents the impactor were modeled as discrete rigid bodies. Figure 1 shows the assembled finite element model. Approximately 5000 4-noded linear quadrilateral explicit shell element of type S4R were used for the column. For the rigid bodies, 2 4-noded rigid linear quadrilateral elements of type R3D4 were used. For

the slotted columns, due to their more complicated geometry, approximately 7000 to 9000 4-noded linear quadrilateral explicit shell elements of type S4R were used.

The slotted column geometric parameters and dimensions are given in Figure 2 and Table 1. Selection of test specimen dimensions is usually dictated by the test rig load capacity. In this case, selection of the test specimens dimension was based on previous work by Zhang, X.W. et al. [7]. Calibration of simulation with previous experimental results is performed to ensure confidence and validity of the proposed analysis technique.

Material properties were assigned to the model. The column is made from aluminium alloy AA6063-T5 [7] and follows the material relationship of elastic-plastic linear strain hardening. Detailed material properties of the column are given in Table 2.

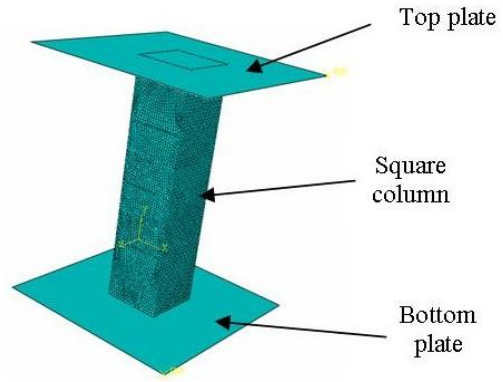

Figure 1: Assembly of Finite Element Models

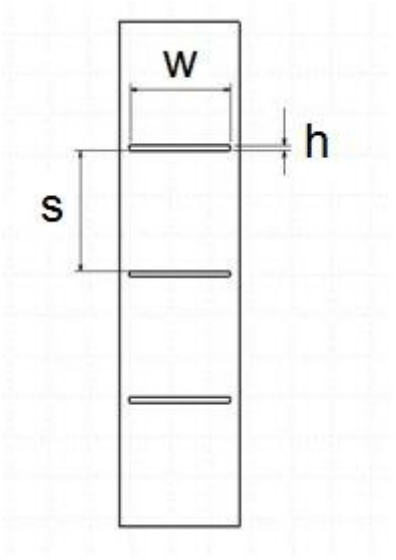

Figure 2: Slotted Column Configuration

Table 1: Dimension of Slotted Column

	Specimen ID		
	S1	S3	S5
Column length (mm)	250	250	250
Column width (mm) and depth (mm)	44.4	44.4	44.4
Column thickness (mm)	1.25	1.25	1.25
Slot length, w (mm)	20	20	20
Slot width, h (mm)	2	2	2
No. of slots	1	3	5
Distance between slots, s (mm)	-	62.5	42

Table 2: Properties of Aluminium Alloy AA6063-T5 [7]

Density	2700 kg/m^3
Ultimate tensile strength (UTS)	220 MPa
Yield strength	180 MPa
Young's Modulus	65 GPa
Poisson's Ratio	0.3
Plastic strain at UTS	0.1

A dynamic explicit solver Abaqus was used. Time duration of 0.02 s to 0.035 s was specified depending on the speed of the impactor. The contact behavior between the column, support and impactor during collision was set up under the interaction module. The contact property consisted of tangential behavior, which used a 'penalty' friction formulation with a coefficient of 0.25. The normal behavior use the 'hard contact' formulation to allow separation after contact. A general dynamic (explicit) contact was utilized where all the contact surfaces are automatically identified by the system.

Boundary conditions and impact speeds were specified in the load module. For the impactor, the boundary conditions were V1=V3=VR1=VR2=VR3=0, which implies that it could only move translationally in the vertical z-direction. The support was fully constrained. The bottom edges of the column were constrained in the z-direction only. Movements in the x- and y-directions were restrained by the friction between the column and the support and impactor. Impactor velocity was specified in the predefined field. The simulation test parameters for calibration are given in Table 3. All specimens will be subjected to impact velocity of 5 m/s to 15 m/s with drop mass of 40 kg.

Table 3: Simulation Test Parameters for Validation

Specimen ID	Mass (kg)	Impact speed (m/s)	Time duration (s)
PS	-	0 (static)	-
PD	68	7	0.03

Results and Discussion

Simulation Validation

Figure 3(a) shows the experimental quasi-static force-displacement curve for plain square column (specimen PS) [7] and Figure 3(b) shows the simulation force-displacement curve. Quasi static means inertia has no effect on the response of the column due to the very low speed whereas in dynamic, inertia effect would be more prominent . The simulation result compared favourably with the experimental result, hence validating the accuracy of the Abaqus explicit code. The simulation was able to predict accurately the IPF, the mean force and the number of folds. Figure 4(a) show the experimental dynamic force-displacement curve for the plain square column (specimen PD) [7] and Figure 4(b) shows the simulation curve. For the dynamic case, the simulation result also compared favourably with the experimental result.

However, the simulation slightly underpredicted the peak force while the mean load and the curve characteristic remained similar. The high experimental peak force was due to stress waves propagation in the specimen during impact[7].

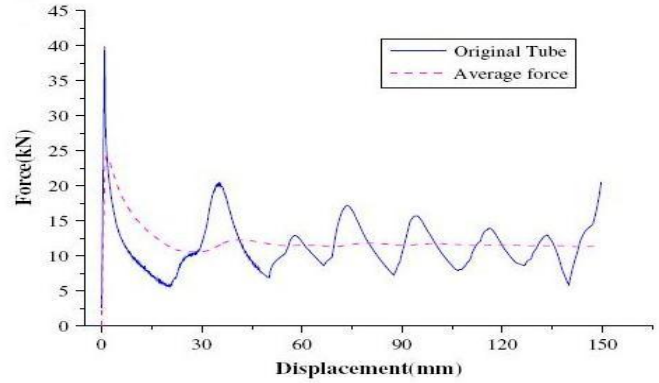

(a)

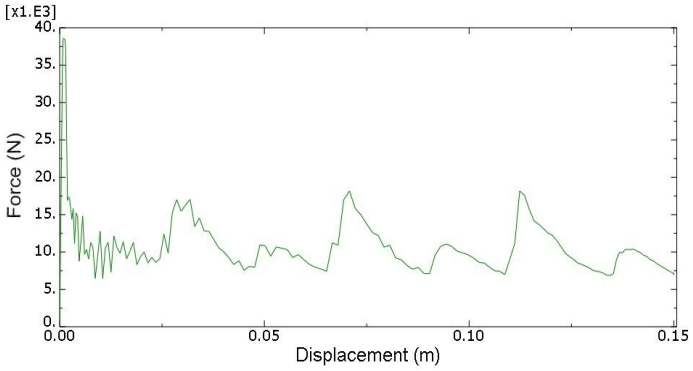

(b)

Figure 3: Quasi-static force-displacement curves: (a) Experimental [7], and (b) simulation

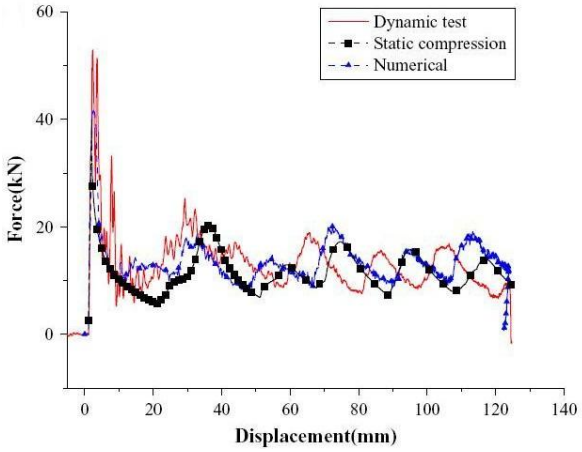

(a)

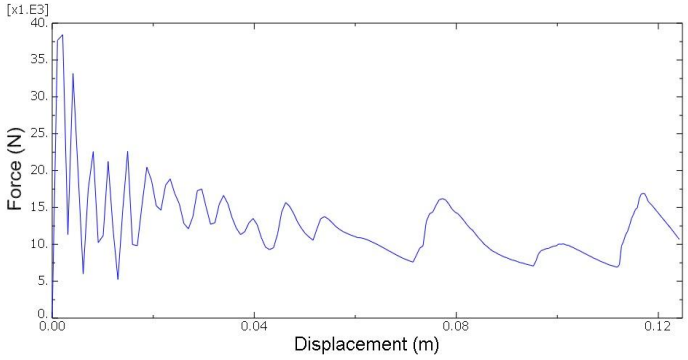

(b)

Figure 4: Dynamic force-displacement curves: (a) Experimental [7], and (b) simulation

Figure 5 shows the quassi-static force-displacement curves for both plain (specimen PS) and 3-slotted (specimen S3) columns. It can be seen that the 3-slotted column showed a considerable decrease in IPF as compared to the plain column. After the formation of the first fold, the 3-slotted column also showed a smoother response. Mean forces for both columns remained the same. Initially, it was believed that the reduction of the column stiffness due to the addition of slots accounted for the lower IPF. However, subsequent simulation results have shown that there was no correlation between the number of slots and reduction of initial peak force.

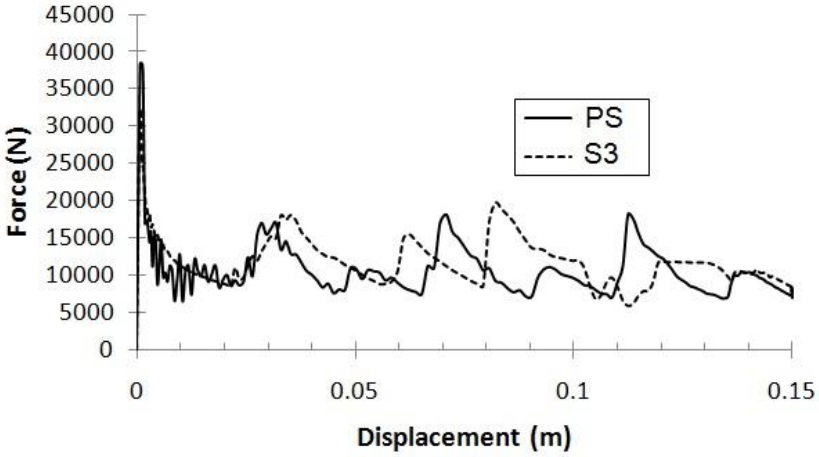

Figure 5: Quassi-static Force-Displacement Curves for Specimen PS (Plain) and Specimen S3 (3-Slotted Column)

Response of Plain Column (Specimen PD)

Figure 6 shows the force-displacement curves for specimen PD subjected to different impact speeds. Figure 7 shows the simulated deformed shapes of the plain columns. The deformation follows the Wierzbicki and Abramowic [8] analytical model. It can be seen that the plain columns exhibited high IPFs followed by lower fluctuating mean forces. The lowest IPF on the plain column was recorded for an impact speed of 15 m/s. The high force toward the end of the travel indicated that the column has bottomed out. Specimen PD failed in progressive buckling mode for all impact speeds. Folding of the sides initiated at the bottom end of the column and progressively moved up to the top of the column. Possible reason for this could be due to the bottom edge having lower friction as compared to the top edge, hence allowing the faces to fold more readily.

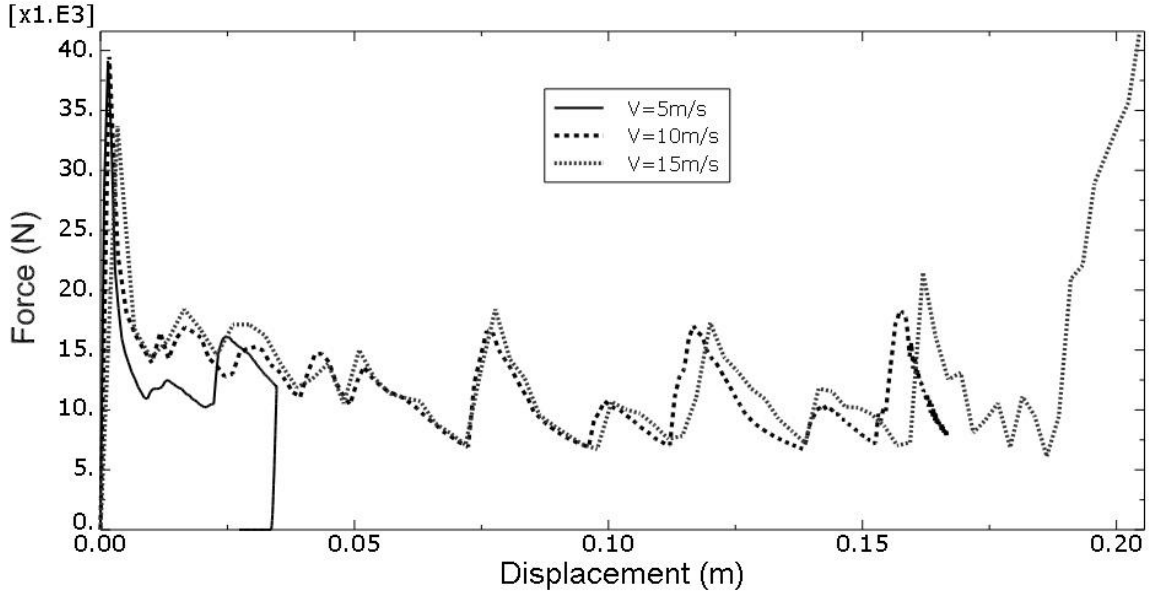

Figure 6: Force-Displacement Curves of Specimen PD for Different Impact Speeds

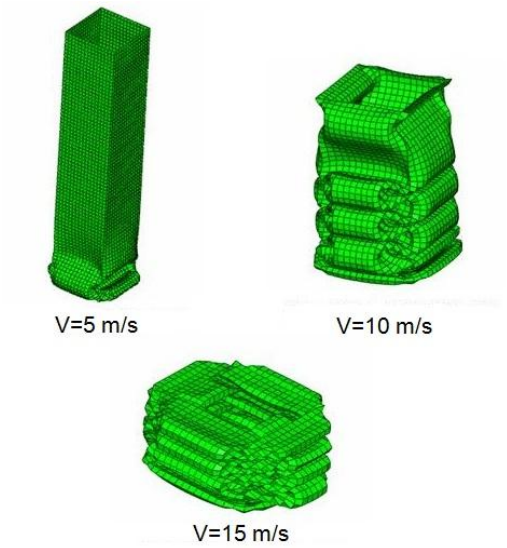

Figure 7: Simulated deformed shapes of specimen PD subjected to different impact speeds

Response of 1-Slotted Column (Specimen S1)

Figures 8 shows the force-displacement curves for the specimen S1 subjected to different impact speeds. All specimens exhibited similar high IPFs followed by lower fluctuating mean forces. The lowest IPF occurred at an impact speed of 10 m/s while the highest occurred at an impact speed of 5 m/s. It can also be seen that at impact speed of 15 m/s, the second high peak force occurred at crushing distance of 0.113 m. Figure 9 shows the simulated deformed shapes of specimen S1. All specimens exhibited progressive buckling failure. Plastic folding initiated at the slot and then propagated to the bottom of the column. Upon complete folding of the bottom half, folding continued to the top half. It can be seen the number of folds was not affected by the number of slot. Number of folds was the same as specimens PD and S3.

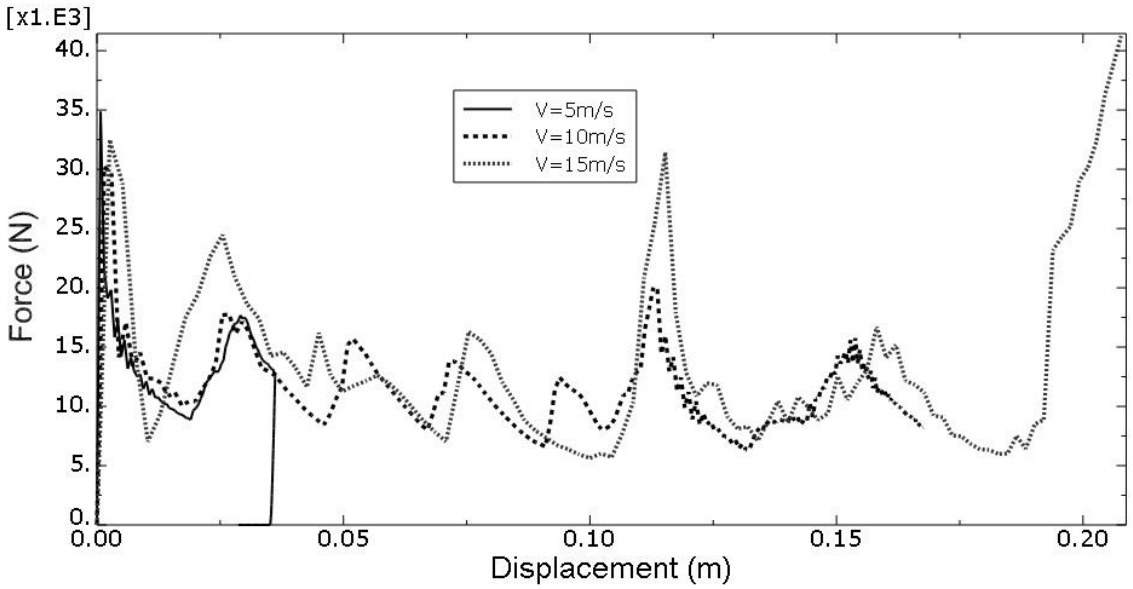

Figure 8: Force-Displacement Curves of Specimen S1 for Different Impact Speeds

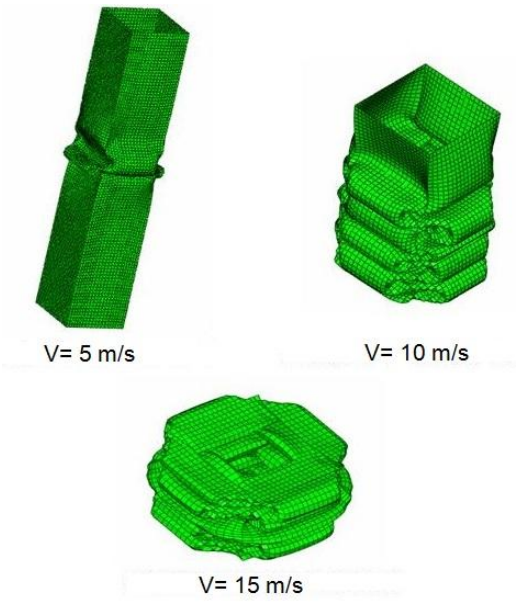

Figure 9: Simulated deformed shapes of specimen S1 subjected to different impact speeds

Response of 3-Slotted Column (Specimen S3)

Figure 10 shows the force-displacement curves for specimen S3 subjected to different impact speeds. Figure 11 shows the simulated deformed shape of the columns. Similiarly, specimen S3 exhibited high IPF followed by lower fluctuating mean forces. The column with impact speed of 15 m/s exhibited the lowest IPF. The high force toward the end of the travel indicated that the column has bottomed out. All specimens failed in progressive buckling mode for all impact speeds. Plastic folding initiated at the slot in the middle of the column and progressively moved up to the top of the column. For a column with imperfection under compression, the first buckling mode is due to formation of plastic hinge in the middle section. The inclusion of slot in the middle section further facilitates the folding of the column sides. Upon complete folding of the top half, folding then continued to the bottom half of the column.

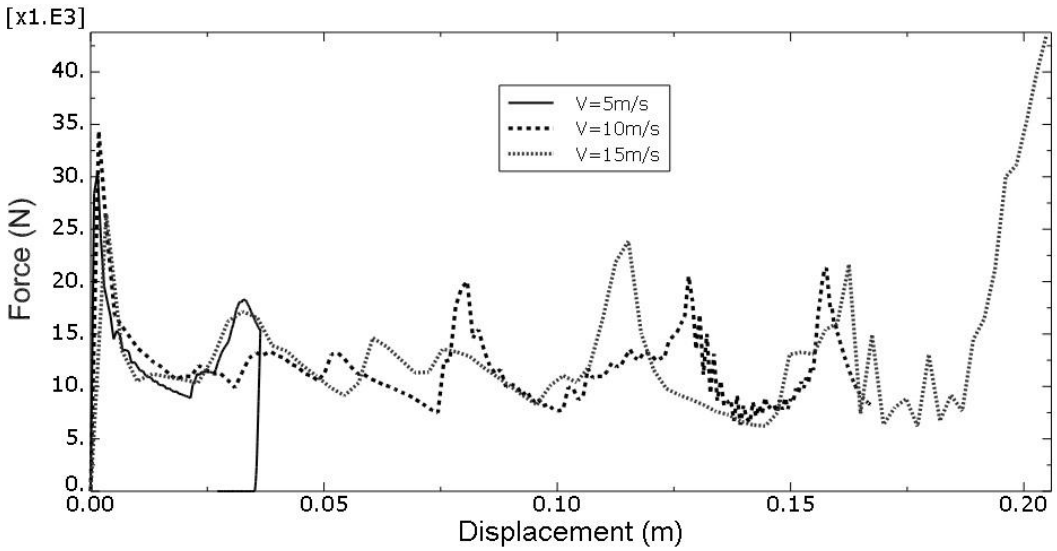

Figure 10: Force-Displacement Curves of Specimen S3 for Different Impact Speeds

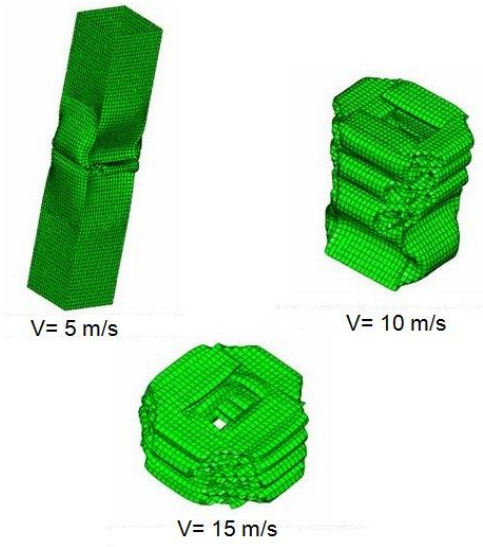

Figure 11: Simulated deformed shapes of specimen S3 subjected to different impact speeds

Response of 5-Slotted Column (Specimen S5)

Figures 12 shows the force-displacement curves for specimen S5 subjected to different impact speeds. All specimens exhibited similar high IPFs followed by lower fluctuating mean forces. The lowest IPF occurred at an impact speed of 5 m/s. Impact speeds of 10 m/s and 15 m/s both gave the same maximum IPFs. Figure 13 shows the simulated deformed shapes of specimen S5. All specimen exhibited progressive buckling failure. At an impact speed of 5 m/s, failure was initiated at the slot in the middle of the column and propagated to the top half. At impact speeds of 10 m/s and 15 m/s, failure initiated at the middle slot and propagated to the bottom half of the column. Upon complete crushing of the bottom half, failure progressed to the top half. The slots in the 5-slotted column acted as guides for the formation of the plastic hinges, giving it a more uniform progressive buckling mode.

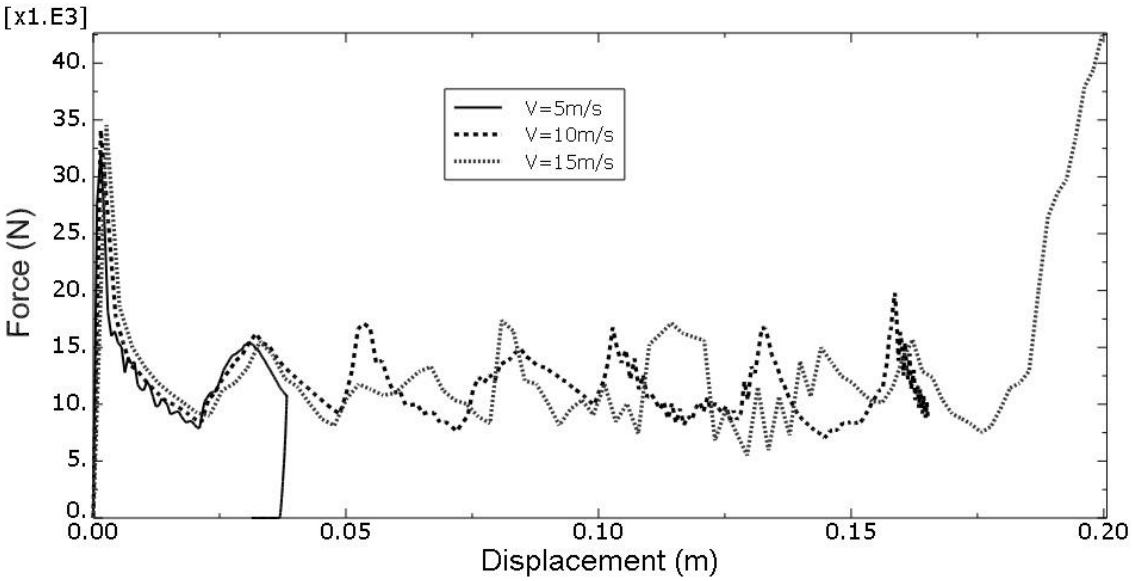

Figure 12: Force-Displacement Curves of Specimen S5 for Different Impact Speeds

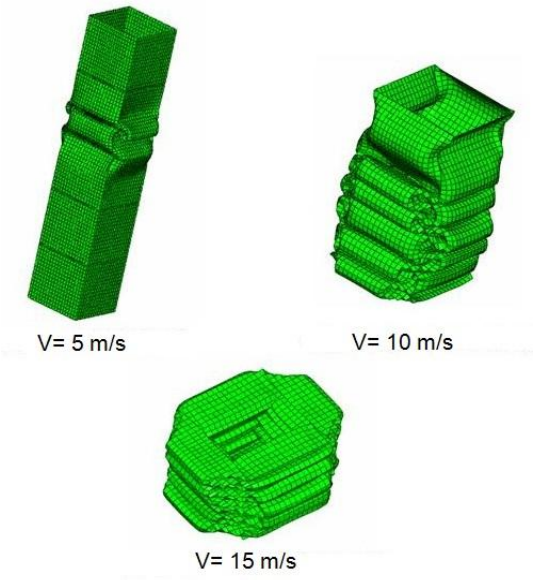

Figure 13: Simulated deformed shapes of specimen S5 subjected to different impact speeds

Comparison Between Specimens at Impact Speed of 5 m/s

Figure 14 shows the force-displacement curves for all specimens subjected to impact speed of 5 m/s. Specimen S3 exhibited the lowest IPF while the specimen PD has the highest IPF, as expected. Despite having lower stiffness as compared to specimen S3, specimen S5 has a slightly higher IPF. Due to the high IPF and slightly higher mean force, specimen PD has the shortest crushing distance. Specimen S5 has the longest crushing distance. All specimens exhibited gradual increase in force after crushing distance of 0.02 m. At the end of the crush travel, slight rebound of the impactor was observed for all specimens, indicating that not all kinetic energy of the impactor was fully absorbed by the specimens. This may imply that a structure which is designed to absorb impact energy at high speed might not be so effective at a much lower speed.

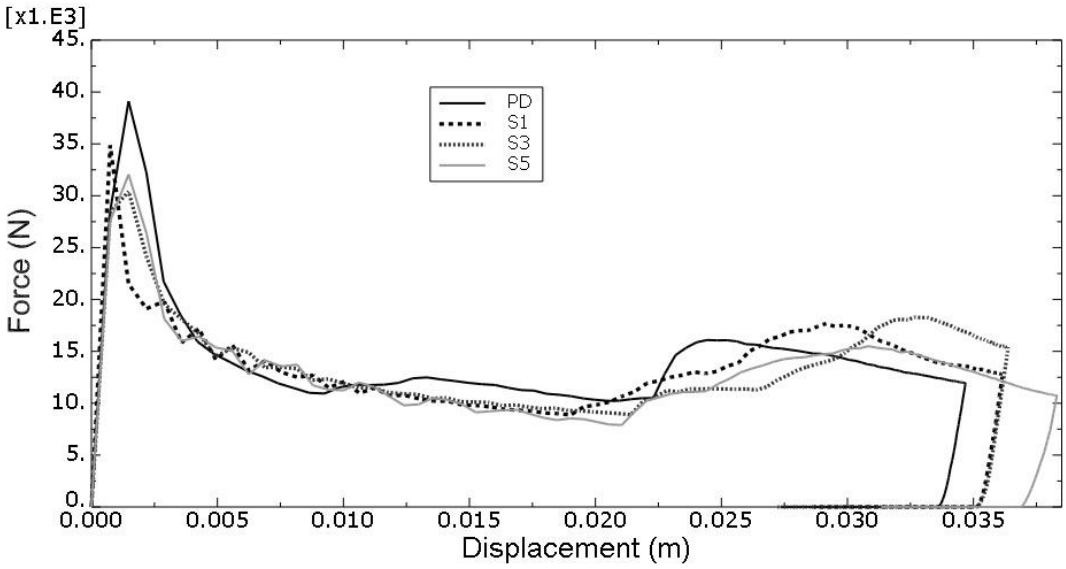

Figure 14: Force-Displacement Curves for All Specimens at Impact Speed of 5 m/s

Comparison Between Specimens at Impact Speed of 10 m/s

Figure 15 shows the force-displacement curves for all specimen subjected to impact speed of 10 m/s. At this speed, specimen S1 exhibited the lowest IPF, followed by specimen S3 and S5. Specimen PD again exhibited the highest IPF. Mean forces and crushing distances for all specimens were similiar despite all specimens having different stiffness. This result may imply that the reduction of IPF is not directly proportional to increased number of slots in the specimen. For this case, one slot is sufficient to provide the lowest IPF while adding more slots would not decrease the IPF further. Specimen PD seemed to have a more smoother response compared to other specimens at higher displacement.

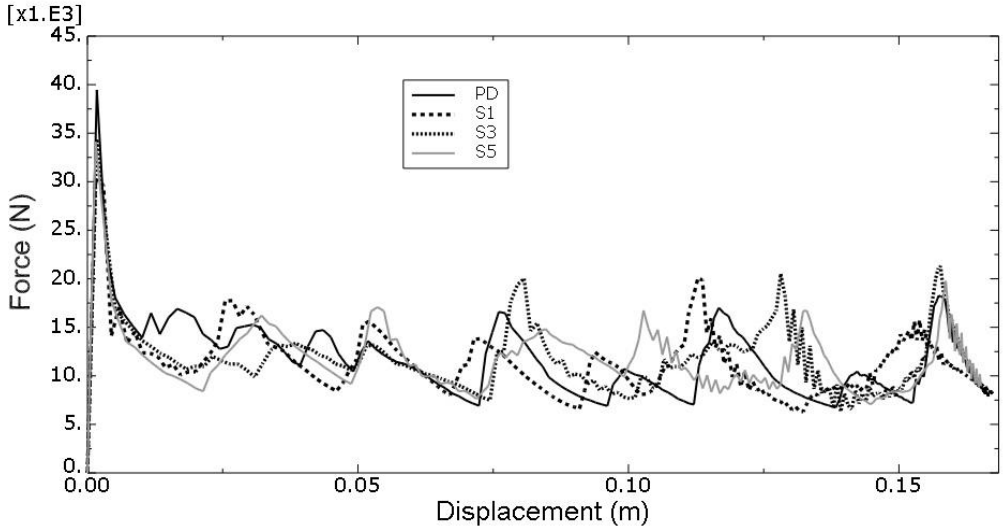

Figure 15: Force-Displacement Curves for All Specimens at Impact Speed of 10 m/s

Comparison Between Specimens at Impact Speed of 15 m/s

Figure 16 shows the force-displacement curves for spcimens subjected to impact speed of 15 m/s. Specimen S3 exhibited the lowest IPF. Surprisingly, both specimens S1 and S5 exhibited IPFs which were equivalent to specimen PD. This

would imply at higher impact speeds, certain number of slots actually have no effect on the reduction of IPF. The results indicate that an optimum number of three slots provided the greatest energy absorption at an impact speed of 15 m/s. This finding suggests that for every impact speed, there will be an optimum number of slots to efficiently absorb the impact energy with the lowest IPF. Mean forces for all specimens were similiar throughout the crush travel except for the specimen S1 where there seemed to be another high peak force which was almost equal to the IPF at a crush distance of about 0.115 m. All specimens bottomed out at crush distance of about 0.19 m.

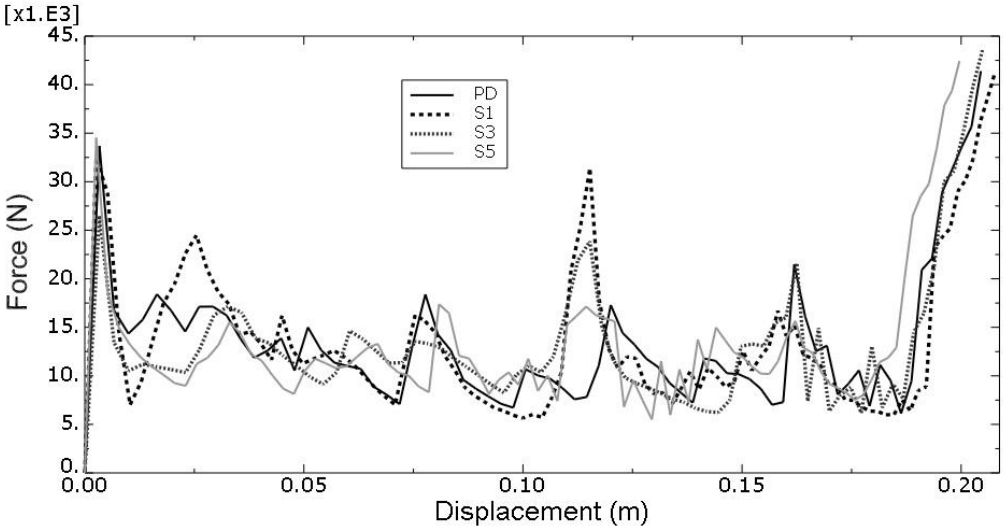

Figure 16: Force-Displacement Curves for All Specimens at Impact Speed of 15 m/s

Comparison of IPF, SEA and CFE

Figure 17 shows that for impact speed of 5 m/s, increasing the number of slots decreased the IPF. However, increasing the number of slots to five slightly increased the IPF. For impact speed of 10 m/s, adding one slot reduced the IPF. Increasing the number of slots to three and five caused the forces to increase again. For impact speed of 15 m/s, increasing the number of slots decreased the IPF. Further increasing the number of slots to five resulted in an increase of IPF which is even higher as compared to the specimen PD. Figure 18 shows that the SEA for all specimens were more or less the same for the same impact speeds. For impact speed of 10 m/s, there was a slight increase in SEA with increased number of slots. For impact speed of 15 m/s, specimen S1 showed a slight reduction in SEA. Further increasing the number of slots gradually increased the SEA. It can be deduced that generally, the inclusion of slots does not substantially affect the amount of energy absorbed. Instead, it has a more prominent effect on how energy is being absorbed. Figure 19 shows that for impact speeds of 5 m/s and 15 m/s, CFE increased with increase number of slots. However, further increasing the number of slots to five resulted in a decrease in CFE. For impact speed of 10 m/s, the inclusion of a single slot increased the CFE. The addition of more slots reduced the CFE but it was still higher as compared to the specimen PD. In most cases, high CFE corresponds to low IPF and vice versa.

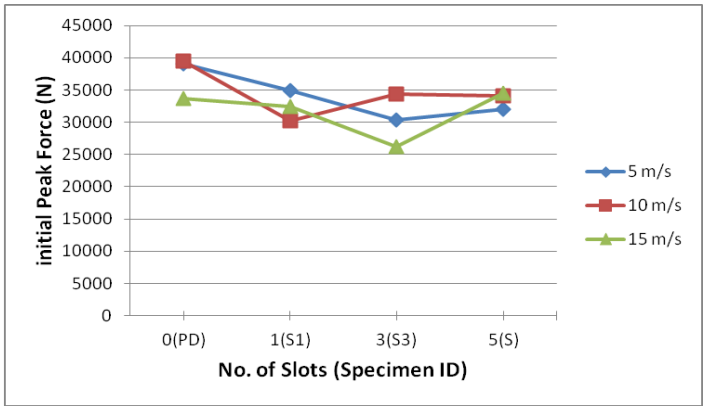

Figure 17: Initial Peak Forces (IPF) for All Specimens at Different Impact Speeds

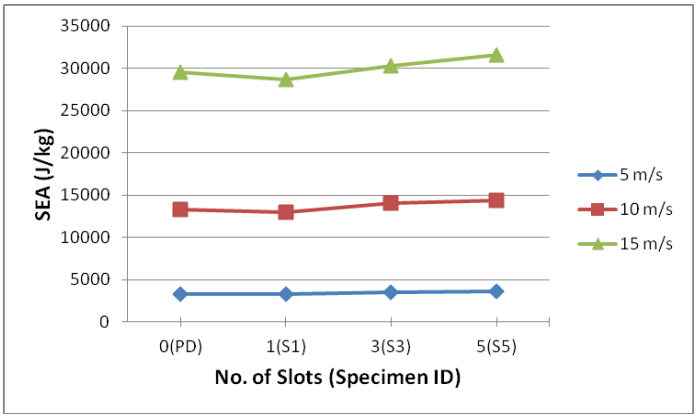

Figure 18: Specific Energy Absorption(SEA) for All Specimens at Different Impact Speeds

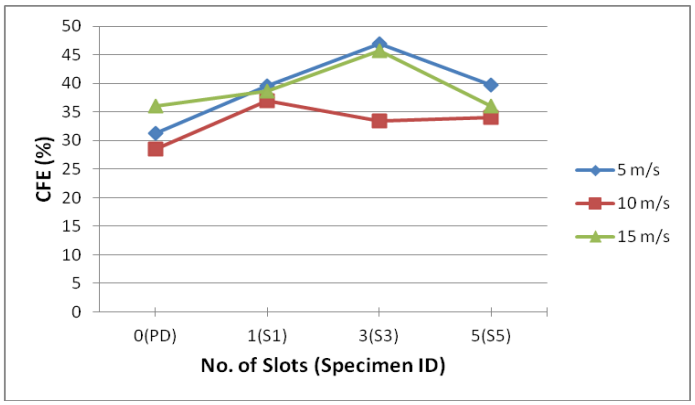

Figure 19: Crush Force Efficiency (CFE) for All Specimens at Different Impact Speeds

Conclusions

This study has shown that slotted column with certain number of slots gives the lowest IPF and highest CFE at certain impact speed. There is no direct correlation between the IPF, SEA, CFE and the number of slots. For every impact speed, there would be a specific number of slots that gave the best impact response. At impact speeds of 5 m/s and 15 m/s, specimen S3 gave the lowest IPF and highest CFE. At impact speed of 10 m/s, specimen S1 has the lowest IPF and highest CFE. Specimen S5 seemed to be less effective in reducing the IPF, despite having lower stiffness and more uniformed crush deformation.

This work demonstrates the possibilities of modifying the impact response of a column by including number of slots on the selected faces of the structure. It is believed that the structure impact performance over a wide range of impact speeds, loads and directions can be improved by the use of this method. Therefore, a more detailed and systematic investigation on parameters such as width and height of slot, spacing between slots, and shape and arrangement of slots, will be carried out in the near future.

References

[1] Johnson, W. (1996). Introduction to Crashworthiness. *International Journal of Crashworthiness*. 1(1): pp 5-10

[2] Jones, N. (1997). Structural Impact. Cambridge University Press.

[3] Yu, T. X. and Lu, G. (2003). Energy Absorption of Structures and Materials. Woodhead Publishing, Cambridge, United Kingdom.

[4] Zhang, X. and Cheng, G. (2007). A Comparative Study of Energy Absorption Characteristics of Foam Filled and Multi Square Columns. *International Journal of Impact Engineering*. 34: pp. 1739-1752.

[5] Daneshi, G.H. and Hosseinipou, S.J. (2003). Grooves Effect on Crashworthiness Characteristics of Thin Walled Tubes Under Axial Compression. *Materials and Design.* 23: pp.611-617.

[6] Zhang, W., Cheng, G. and Zhang, H. (2009). Numerical Investigation on a New Type of Energy Absorbing Structure Based on Free Inversion of Tubes. *International Journal of Mechanical Sciences*. 51: pp.64-76.

[7] Zhang, X.W., Su, H. and Yu, T.X. (2009). Energy Absorption of an Axially Crushed Square Tube with a Buckling Initiator. *International Journal of Impact Engineering*. 36: 402-417.

[8] Wierzbicki, T and Abramowicz, W. (1983). On the Crushing Mechanics of Thin Walled Structures. *Journal of Applied Mechanics*. 50(4a): pp727-734.

.